J Neurophysiol 98: 2992–3005, 2007.
First published September 5, 2007; doi:10.1152/jn.00877.2007.

A Central Pattern Generator Producing Alternative Outputs: Pattern, Strength, and Dynamics of Premotor Synaptic Input to Leech Heart Motor Neurons

Brian J. Norris,[1,2,*] Adam L. Weaver,[1,*] Angela Wenning,[1] Paul S. García,[1] and Ronald L. Calabrese[1]
[1]*Department of Biology, Emory University, Atlanta, Georgia; and* [2]*Department of Biological Sciences, California State University, San Marcos, California*

Submitted 7 August 2007; accepted in final form 3 April 2007

Norris BJ, Weaver AL, Wenning A, García PS, Calabrese RL. A central pattern generator producing alternative outputs: pattern, strength, and dynamics of premotor synaptic input to leech heart motor neurons. *J Neurophysiol* 98: 2992–3005, 2007. First published September 5, 2007; doi:10.1152/jn.00877.2007. The central pattern generator (CPG) for heartbeat in medicinal leeches consists of seven identified pairs of segmental heart interneurons and one unidentified pair. Four of the identified pairs and the unidentified pair of interneurons make inhibitory synaptic connections with segmental heart motor neurons. The CPG produces a side-to-side asymmetric pattern of intersegmental coordination among ipsilateral premotor interneurons corresponding to a similarly asymmetric fictive motor pattern in heart motor neurons, and asymmetric constriction pattern of the two tubular hearts, synchronous and peristaltic. Using extracellular recordings from premotor interneurons and voltage-clamp recordings of ipsilateral segmental motor neurons in 69 isolated nerve cords, we assessed the strength and dynamics of premotor inhibitory synaptic output onto the entire ensemble of heart motor neurons and the associated conduction delays in both coordination modes. We conclude that premotor interneurons establish a stereotypical pattern of intersegmental synaptic connectivity, strengths, and dynamics that is invariant across coordination modes, despite wide variations among preparations. These data coupled with a previous description of the temporal pattern of premotor interneuron activity and relative phasing of motor neuron activity in the two coordination modes enable a direct assessment of how premotor interneurons through their temporal pattern of activity and their spatial pattern of synaptic connectivity, strengths, and dynamics coordinate segmental motor neurons into a functional pattern of activity.

INTRODUCTION

Central pattern generator (CPG) networks (De Schutter et al. 2005; Marder and Calabrese 1996; Marder et al. 2005), consisting mainly of interneurons, must distribute their output over an ensemble of motor neurons to control rhythmic behavior. When the muscles that are controlled are segmentally distributed, as in those producing whole body undulatory waves (Hill et al. 2003), the motor neuron ensemble is also segmentally distributed, and motor neurons in different segments must be coordinately controlled to produce effective movement. Much progress has been made in qualitatively defining the neuronal composition and synaptic connectivity patterns of several CPG networks. However, the activity of these networks likely depends not only on the pattern of synapses in the network, but also on the strengths of these connections. Furthermore, many synapses show use-dependent changes in synaptic strength (e.g., facilitation), which would also be expected to affect network activity. Understanding network activity on the cellular level thus requires quantitative measurements of both the strengths of the network's synapses and of how these strengths vary with network output phase (Marder et al. 2005).

In invertebrates, and especially in the stomatogastric nervous system of crustaceans, there have been efforts to determine the strength and plasticity of outputs onto motor neurons and to use this information in constructing computational models that can illuminate mechanisms of motor neuron coordination (Mamiya and Nadim 2005; Rabbah and Nadim 2005). Although the utility of the stomatogastric nervous system in analyzing circuit dynamics and modulation is unrivaled (Marder and Bucher 2007), it is not well suited to illuminate intersegmental coordination because of its inherent centralization. Other similar efforts have focused on reflexes that are restricted to one or a few segments, such as leech local bend reflexes (Kristan et al. 1995, 2005; Lockery and Kristan 1990a,b) and locust wing reflexes (Burrows 1975a,b,c) and steering movements (Burrows and Pfluger 1992; Pfluger and Burrows 1990).

Although much progress is now being made identifying the key neuronal elements that make up vertebrate pattern generators, assessments of synaptic strengths and dynamics are lacking. Only a few vertebrate systems are described well enough to allow the construction of computational models that generate specific hypotheses about motor neuron coordination (Butera et al. 1999a; b; Del Negro et al. 2001; Kotaleski et al. 1999a,b; Rybak et al. 2004a,b; Sautois et al. 2007; Tunstall et al. 2002). A notable exception are vestibulo- and reticulospinal projection interneurons that coordinate attitude adjustments and turning during swimming in lampreys (Deliagina et al. 2002; Zelenin et al. 2001, 2003, 2007). In this system, the considerable effort at determining the synaptic strength of connections onto motor neurons has been fruitful; nevertheless the output of these interneurons may be viewed as having a tonic effect to adjust the balance of motor outflow without affecting its dynamics or intersegmental coordination.

One of our long-range aims is a complete model of how a CPG controls intersegmental motor outflow. Here we focus on a quantitative assessment of synaptic strength and dynamics and associated conduction delays of intersegmental premotor interneurons that coordinate motor neuron activity into a fictive motor pattern. Nevertheless, problems arise as to useful metrics for model network construction and internetwork comparison.

* These authors contributed equally to this work.

Address for reprint requests and other correspondence: R. L. Calabrese, Dept. of Biology, Emory University, 1510 Clifton Road N.E., Atlanta, GA 30322 (E-mail: ronald.calabrese@emory.edu).

The costs of publication of this article were defrayed in part by the payment of page charges. The article must therefore be hereby marked "*advertisement*" in accordance with 18 U.S.C. Section 1734 solely to indicate this fact.

Neuronal networks, and CPGs in particular, can display a two- to fivefold range of intrinsic membrane currents and synaptic strengths while still producing stereotypical output (Marder and Goaillard 2006). Moreover, there are indications that average values for such strength parameters may be misleading, in that models constructed from average values may not produce stereotypical output (Golowasch et al. 2002; Haedo and Golowasch 2006). We argue here that for intersegmental comparisons averages are useful metrics, but we also provide key data on animal-to-animal variability.

Motor pattern generating networks can produce motor variants that reflect changes in coordination between motor elements necessary for opposing functions, as for example egestive versus ingestive biting behavior in the mollusk *Aplysia* (Cropper et al. 2004; Hurwitz and Susswein 1996). Although it is widely appreciated that such alternative forms of network output require changes in the activity phase of key premotor interneurons within the CPG, concomitant changes in synaptic strength and dynamics of synaptic inputs to motor neurons have not been widely explored. Here we attempt to resolve whether such changes in networks motor output are reflected by changes in synaptic strengths and dynamics.

The heartbeat control system of the medicinal leech is described in the INTRODUCTION of the companion paper (Norris et al. 2007). Figure 1*A* summarizes the connectivity between premotor interneurons of the heartbeat CPG and motor neurons in this system. Here we provide the missing quantitative assessment of the strength and dynamics, and associated conduction delays of premotor interneuron synaptic output onto the entire ensemble of segmental heart motor neurons. We also assess synaptic strength across switches in coordination mode and we describe the animal-to-animal variability in the synaptic strength and use it to assess the functional relevance of the view that emerges from average data.

METHODS

Animals and solutions

Leeches (*Hirudo* sp) (Siddall et al. 2007) were obtained from commercial suppliers (Leeches USA, Westbury, NY and Biopharm, Charleston, NC) and maintained in artificial pond water at 15°C. After the animals were anesthetized in cold saline, chains of ganglia were dissected consisting of the head brain (HB) to at least midbody ganglion 15 (G15) for recording the heart interneuron activity rhythm and G2 to G8 for recording the HN(X) heart interneuron inhibitory postsynaptic current (IPSC) pattern in heart motor neurons. Extra ganglia were in some cases left attached to these later preparations for pinning purposes but the connectives to these ganglia were thoroughly crushed. The preparations were pinned (ventral surface up) in 60-mm petri dishes lined with Sylgard (Dow Corning, Midland, MI). Ganglia in which heart interneurons or heart motor neurons were to be recorded were desheathed using fine scissors or microscalpels [in the few cases when HN(X)-mediated IPSCs were recorded in HE(5) or HE(6) motor neurons, ganglia were not desheathed]. The preparation was superfused continuously with normal leech saline containing (in mM): 115 NaCl, 4 KCl, 1.8 $CaCl_2$, 10 glucose, 10 HEPES buffer, adjusted to pH 7.4 with NaOH, at 1–2 ml/min (bath volume 6–8 ml). Heart motor neurons and interneurons were identified based on soma size, soma location in the ganglion, and ultimately identified by their characteristic bursting activity (e.g., Fig. 2). Previous experience has indicated that the heart interneuron HN(X) activity pattern associated with synchronous coordination is sensitive to prolonged dissection and extensive desheathing of ganglia (Norris et al. 2006); thus when recording HN(X) heart interneuron's IPSCs, or the coordination of front motor neurons with premotor interneurons all attempts were made to keep dissections <1 h and to minimize the number of ganglia desheathed. Moreover, those preparations where the HN(X) heart interneuron inhibitory postsynaptic potential (IPSP) pattern or the phasing of front motor neurons never switched out of the peristaltic state during the course of an experiment (often despite documented switches in the identified rear premotor interneurons) were discarded.

Extracellular and intracellular recording techniques

For intracellular voltage and voltage-clamp recordings from heart motor neurons, we used sharp intracellular electrodes (~20–30 MΩ filled with 4 M KAc, 20 mM KCl) following the methods described in Opdyke and Calabrese (1995). Briefly, intracellular recordings were performed using an Axoclamp-2A amplifier (Axon Instruments, Union City, CA) operating in discontinuous current-clamp or discontinuous single-electrode voltage-clamp mode with a sample rate of 2.5–2.8 kHz. The electrode potential was monitored to ensure that it settled during each sample cycle. Output bandwidth was 0.3 kHz. Voltage-clamp gain was 0.8 to 2.0 nA/mV. The voltage-clamp holding potential for recording spontaneous IPSCs in motor neurons was −45 mV in all experiments except those involving recording HN(X)-mediated IPSCs, where it varied from −35 to −55 mV in an attempt to minimize escape spiking while maximizing IPSC amplitude. At the end of each experiment the electrode was withdrawn from the motor neuron and only data in which the electrode potential was within ±5 mV of ground were included. Thus holding potentials were accurate within ±5 mV.

For extracellular recordings from heart interneurons, we used suction electrodes filled with normal saline. Electrodes were pulled on a Flaming/Brown micropipette puller (P-97, Sutter Instrument, Novato, CA) from borosilicate glass (1 mm OD, 0.75 mm ID; AM Systems, Carlsborg, WA) and placed in a suction electrode holder (E series, Warner Instruments, Hamden, CT). To ensure a tight fit between the cell and electrode, the electrode tips had a final inner diameter of about 20 μM, approximately the diameter of a heart interneuron's soma. The electrode tip was brought in contact with the cell body and light suction was applied using a syringe until the entire cell body was inside the electrode. Extracellular signals were monitored with a differential AC amplifier (model 1700, AM Systems) at a gain of 1,000 with the low- and high-frequency cutoffs set at 100 and 1,000 Hz, respectively. Noise was reduced with a 60-Hz notch filter and a second amplifier (model 410, Brownlee Precision, Santa Clara, CA) amplified the signal appropriately for digitization.

Data acquisition and analysis

Data were digitized (3.3-kHz sampling rate) using a digitizing board (Digi-Data 1200 Series Interface, Axon Instruments, Foster City, CA) and acquired using pCLAMP software (Axon Instruments) on a personal computer (PC).

Determining the identified heart interneuron to heart motor neuron connectivity pattern, synaptic strength and dynamics, and conduction delays

To determine the strength, dynamics, and conduction delays of each inhibitory synaptic connection from a premotor heart interneuron to a segmental heart motor neuron, we recorded extracellularly from two ipsilateral identified premotor interneurons (one rear and one front to determine coordination mode of the CPG). We then voltage clamped an ipsilateral segmental series of heart motor neurons (−45-mV holding potential) one after another, recording spontaneous IPSCs for several interneuron burst cycles in each, usually spanning both coordination modes. In all, 56 preparations were used exclusively in these

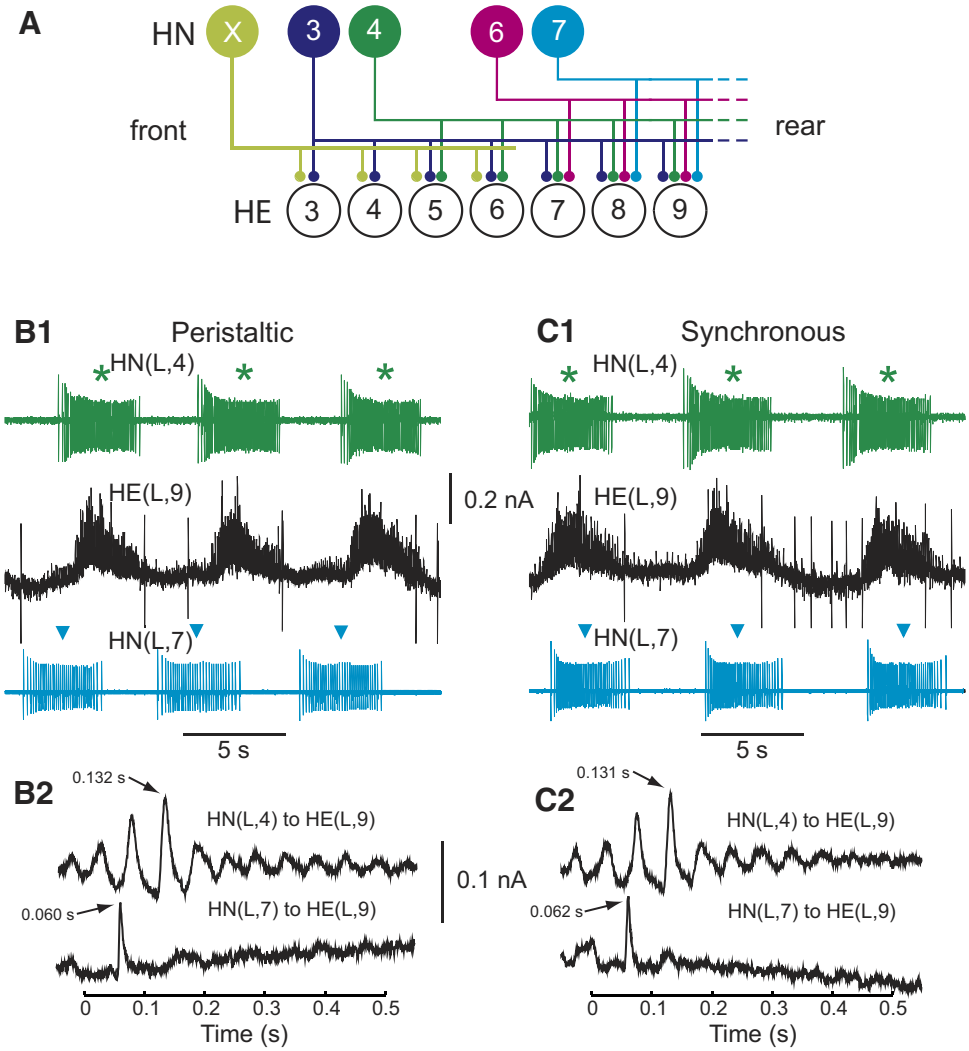

FIG. 1. Establishing the inhibitory synaptic strength of the identified heart interneurons. *A*: hemilateral circuit diagram showing all the premotor heart (HN) interneurons of the central pattern generator (CPG) [identified HN(3), HN(4), HN(6), HN(7), and unidentified HN(X)] and their pattern of synaptic connections to ipsilateral motor neurons (HE) in HE(3)–HE(9). Large colored (heart interneurons from different segments are color coded as in Norris et al. 2007) circles are cell bodies and associated input processes, lines indicate cell processes, and small colored/black circles indicate inhibitory chemical synapses. The HN(X) interneuron is defined as one that gives rise to matched inhibitory postsynaptic potentials (IPSPs) in ipsilateral G3–G6 heart motor neurons and rectifying electrical coupling potentials in ipsilateral G3 and G4 interneurons (Calabrese 1977). *B* and *C*: an HE(L,9) motor neuron was recorded in voltage clamp (holding potential −45 mV) simultaneously with extracellular recording from 2 ipsilateral premotor heart interneurons, HN(L,4) and HN(L,7), in both peristaltic (*B1*) and synchronous (*C1*) coordination mode. Colored asterisks and triangles indicate the middle spike of the HN(L,4) and HN(L,7) bursts, respectively. In both modes (*B2*, peristaltic; *C2*, synchronous) spikes from several bursts from each interneuron were used to generate spike-triggered averages of inhibitory postsynaptic currents (IPSCs) in the motor neuron (see METHODS). For the spike-triggered averages, 0 on the timescale indicates the time of the triggering interneuronal spike and arrows indicate the latency of the peak average IPSC from this triggering event. For most of the duration of their bursts, the premotor interneurons tend to fire at a quasi-constant rate, often resulting in multiple peaks in the spike-triggered average. We reasoned that the largest of these peaks reflected the average of directly elicited IPSCs and not correlated IPSCs and therefore here and subsequently, we chose the largest average IPSC in each trace for measurement of amplitude and latency. The first 5 spikes in a premotor interneuron's burst were excluded in our determination of average synaptic strength because the associated IPSCs were very small (see Fig. 5). Here and throughout, interneurons and motor neurons are indexed by body side (R or L) and segmental ganglion number; thus HN(L,7) is the left heart interneuron of segmental ganglion 7. Peristaltic coordination mode can be recognized when the rear premotor interneurons lead the front interneurons in activity phase (*B1*) and the synchronous coordination can be recognized when the rear premotor interneurons slightly lag the front interneurons in activity phase (*C1*). All records are from the same preparation. Color code is the same as in *A*.

experiments but data from these were supplemented by comparable data from 13 preparations (69 total) that were used in the experiments on HN(X)-mediated input to motor neurons described in the subsequent section. We then used off-line spike-triggered averaging of IPSCs to determine synaptic connectivity, strength, and dynamics in both coordination modes. Data from the two coordination modes were first analyzed separately when possible. Ultimately, because no significant differences were noted between coordination modes in synaptic connectivity, strength, or dynamics, for some analyses, averages were taken combining both coordination modes to increase the number of presynaptic spikes used and thus increase signal to noise in spike-triggered averages.

Spike and IPSC detection/averaging were performed off-line using custom-made MATLAB software (The MathWorks, Natick, MA). For most of the duration of their bursts, the premotor interneurons tend to fire at a quasi-constant rate, often resulting in multiple peaks in the spike-triggered average. We reasoned that the largest of these peaks reflected the average of directly elicited IPSCs and not correlated IPSCs, and therefore we chose the largest average IPSC in each trace for measurement of amplitude and latency. This choice might have led

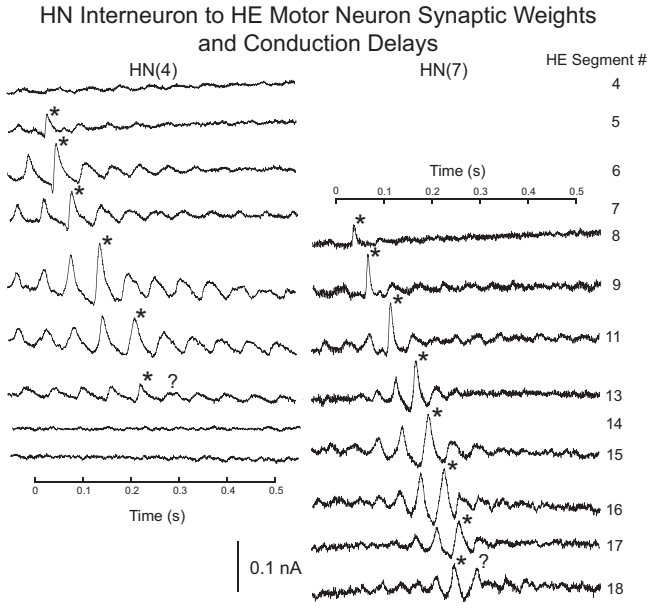

FIG. 2. Spike-triggered average IPSCs in a segmental series of heart motor neurons produced by an ipsilateral HN(4) (*left*) and an ipsilateral HN(7) (*right*) premotor interneuron: *left* and *right panels* from 2 different preparations; 0 on the timescale indicates the time of the triggering interneuronal spike and asterisks indicate the latency of the peak average IPSC from this triggering event. Where the largest IPSC in the spike-triggered average does not correspond to the expected latency a "?" labels an IPSC at the expected latency. Segment number (#) of the HE motor neuron recorded is indicated on *right*.

to some errors as discussed in RESULTS, but it is totally objective. The average strength of a synaptic connection was defined as the amplitude (measured from the preceding baseline current) of the largest peak of the spike-triggered average IPSC from all presynaptic heart interneuron spikes in a burst except the first 5 spikes, for a series of bursts ($n \geq 20$ in all preparations except 4, where $n = 6$). (When making peristaltic and synchronous comparisons, spikes from $n \geq 10$ bursts in each coordination mode were used to generate separate spike-triggered averages. Subsequently, spikes from both modes were combined in a single spike-triggered average for averaging across preparations.) These average strengths were then averaged across a number of different experiments (preparations). In some cases, no detectable synaptic current above noise level was detectable in the spike-triggered average and the average strength for that connection in that preparation was assigned 0. To determine synaptic dynamics, presynaptic heart interneuron spikes were grouped according to spike number from a series of bursts ($n \geq 12$) were grouped according to spike number. Then each spike number group was used separately to generate a spike-triggered average. Thus a spike-triggered average IPSC was generated for each spike in the interneurons burst. In some cases, this procedure was done independently for the two coordination modes for a particular HE motor neuron (e.g., see Fig. 5). All IPSCs were converted to conductances using a reversal potential of −62 mV (Angstadt and Calabrese 1991).

Determining the synaptic strength and dynamics of the HN(X) interneuron to front heart motor neuron synaptic connections

We used an indirect method to identify the postsynaptic currents (IPSCs) elicited by the HN(X) heart interneuron in the HE(3)–HE(6) heart motor neurons as described previously (Norris et al. 2006). In 13 preparations, switching was regular with appropriate and robust changes in phasing of the interneuron HN(X)-mediated IPSCs. We recorded between 2 and 13 switches per experiment analyzed; a minimum of 2 switches with regular intervals had to be observed for data to be recorded and included in the analysis. Briefly, we recorded extracellularly from an ipsilateral HN(4) and/or HN(3) premotor interneuron; coordination mode of the CPG was determined by the IPSC pattern in the motor neuron. We then voltage clamped an ipsilateral HE(3)–HE(6) motor neuron (−35- to −55-mV holding potential), recording spontaneous IPSCs for several cycles, in both coordination modes. Coordination mode of the CPG was determined by the IPSC pattern in the motor neuron. We used 11 to 13 bursts per coordination mode except in the two preparations where we recorded the HE(6) motor neuron. In one of these preparations, we could analyze only 4 cycles in the peristaltic mode and 5 in the synchronous mode, and in the other preparation, we could analyze 12 bursts in the synchronous, but only 6 on the peristaltic mode. Data from the two coordination modes were analyzed separately because there were apparent size differences of the HN(X)-mediated IPSCs in the two coordination modes. From these preparations, we also obtained data on the average strength of a synaptic connection of the HN(3) and HN(4) interneurons to the HE(3)–HE(6) motor neurons to supplement the data from the 56 preparations of the preceding section as described therein.

Spike and IPSC detection were performed off-line using custom-made MATLAB software (The MathWorks) and pCLAMP analysis software in a multistep process. Spike times of the relevant premotor interneurons [HN(3) and/or HN(4)] and the latency between their spike time and the time of the IPSCs in HE(3)–HE(6) heart motor neurons were determined. These values were then used to identify, and graphically display, the IPSCs in the heart motor neuron caused by HN(3) and HN(4) interneuron(s). All other postsynaptic potentials were attributed to the HN(X) interneuron. Next, the time of peak of each IPSC was determined using current traces that were filtered (low-pass, Gaussian) at 70–85 Hz for noise reduction. For interneuron HN(X)-mediated IPSC identification, events less than twice the size of the noise were rejected as were summed IPSCs. In 7 of the 13 preparations, an HE(3) motor neuron was recorded, and in 5 an HE(4) motor neuron was recorded; in 3 preparations, an HE(5) motor neuron was recorded [in one preparation without the HE(3) motor neuron, in 2 preparations together with a HE(3) motor neuron]; and in two preparations an HE(6) motor neuron was recorded together with an HE(3) motor neuron, although in one of these preparations there was too much uncontrolled spike activity in the HE(3) motor neuron to permit accurate detection of HN(X)-mediated IPSCs.

IPSCs and spikes were then grouped into bursts as described in the next section. For spike trains, the same criteria as subsequently described were used, but for bursts of IPSCs we used 0.10 of the respective cycle period as the critical interburst interval. The phase of these bursts with respect to the HN(4) interneurons was previously established (Norris et al. 2006) and these bilateral (absolute) phases were used to reference amplitude histograms (subsequently described) to the heart interneuron activity pattern. The peak amplitude of each identified HN(X)-mediated IPSC was converted into peak current at a −45-mV holding potential or peak conductance using a reversal potential of −62 mV. HN(X)-mediated IPSCs were first binned at 0.05-phase intervals and, in a second step, their respective peak conductances were averaged for each bin, first within and then across preparations for each motor neuron and displayed in an amplitude histogram.

To estimate total graded transmission we used the same bursts as in the previous analysis; the current trace was low-pass filtered at 2 Hz and 11–13 slow-wave cycles per coordination mode were averaged. Due to the filtering used, we overestimated the graded transmission, especially if unclamped spiking occurred. We converted these average currents to conductance by assuming that the minimum outward current represented the leak current at the holding potential used and that all outward current above this level represented graded inhibitory synaptic input. The peak amplitude of the graded transmission was then determined.

Statistics

Means are presented ± SD and, in some cases, the coefficient of variation (CV) is expressed as a decimal fraction of the mean. Conductance and delay measurements were subjected to ANOVA to determine significant differences between effects. The *F* statistic, degrees of freedom (*df*), and *P*-values are reported. Where appropriate, post hoc testing was done with Tukey's HSD test. In cases where ANOVA was not appropriate, we performed paired *t*-tests (two-tailed). For all tests $P < 0.05$ was the criterion for significant difference.

RESULTS

Our present aim was to characterize as quantitatively as possible the pattern, strength and dynamics, and conduction delays of each inhibitory synaptic connection from a premotor heart interneuron to a segmental heart motor neuron to complement our previous quantitative descriptions of the firing pattern and phase relations of the heart interneurons (Norris et al. 2006) and of their phase relations (coordination) with the heart motor neurons, thus fully characterizing the output of the heartbeat CPG. We recorded extracellularly from two ipsilateral identified premotor interneurons (one rear and one front to determine coordination mode of the CPG) while recording synaptic currents in voltage clamp from a series of segmental heart motor neurons. First, we analyzed directly the synaptic output of the identified premotor interneurons onto the HE(3)–HE(18) heart motor neurons, and then we analyzed the synaptic output of the unidentified HN(X) heart interneuron, using indirect methods to identify their IPSCs in HE(3)–HE(6) motor neurons.

Connectivity, synaptic strength, and conduction delays of identified premotor interneurons

The recordings were made with one front premotor interneuron [HN(3) or HN(4) interneuron] and one ipsilateral rear premotor interneuron [HN(6) or HN(7) interneuron], whereas an ipsilateral segmental series of heart motor neurons [HE(3)–HE(18)] were recorded and voltage clamped to reveal spontaneous IPSCs arising from the activity of the recorded and other ipsilateral interneurons. The relative phasing of the rear and front premotor interneurons permitted an unambiguous determination of the coordination mode of the CPG, synchronous or peristaltic. For each motor neuron, we recorded the spontaneous IPSCs for several interneuron burst cycles ($n \geq 20$ in most preparations; see METHODS) spanning both coordination modes. When $n \geq 10$ interneuron bursts were available in each coordination mode, we first analyzed the two modes separately.

Figure 1, *B1* and *C1* illustrates typical voltage-clamp recordings in an HE(9) motor neuron and extracellular recordings of ipsilateral HN(4) and HN(7) premotor interneurons in both coordination modes. Heart interneurons produce both spike-mediated and graded synaptic currents in their postsynaptic targets (Angstadt and Calabrese 1991; Ivanov and Calabrese 2006a,b; Lu et al. 1997). As can be seen in the records illustrated (Fig. 1, *B1* and *C1*) graded transmission, as indicated by the slow wave of current underlying bursts of IPSCs, is not large compared with the spike-mediated IPSCs themselves in heart motor neurons during normal premotor activity. This observation is consistent with analyses of graded transmission between heart interneurons (Olsen and Calabrese 1996; Tobin and Calabrese 2005). As subsequently shown, this observation does not hold for the frontmost segmental motor neurons [the HE(3)–HE(6) motor neurons], which are the targets of the unidentified HN(X) interneurons where graded transmission can be substantial.

Here we focus on spike-mediated synaptic transmission by using spike-triggered averaging of IPSCs as illustrated in Fig. 1, *B2* and *C2*. In the peristaltic mode, the average IPSC in the HE(9) motor neuron elicited by the HN(4) interneuron was larger in amplitude (measured from the preceding baseline current) than that elicited by the HN(7) interneuron (0.15 vs. 0.12 nA) and came at a longer conduction delay (this conduction delay is the time from the triggering spike to the peak of the average IPSC and includes the spike conduction time and the synaptic delay) (132 vs. 60 ms). We always chose the largest peak in the spike-triggered average as reflecting the average of directly elicited IPSCs (see METHODS). This longer conduction delay is commensurate with the delay of about 20–30 ms per segment observed across all recordings of this type (see following text). Indistinguishable results were obtained in the synchronous coordination mode for both amplitude (0.15 vs. 0.12 nA) and conduction delay (131 vs. 62 ms).

In all subsequent analyses, IPSCs were converted to conductances (so that data taken at different holding potentials could be compared) as described in METHODS and henceforth referred to as IPSC amplitude or synaptic strength. Where raw currents are compared in figures, all recordings were at the same holding potential (−45 mV). In 24 different preparations (18 with two premotor interneurons recorded and 6 with a single premotor neuron recorded), the IPSCs evoked by the identified premotor neurons were compared this way [HN(3) 52 comparisons, HN(4) 54 comparisons, HN(6) 26 comparisons, and HN(7) 54 comparisons] in all motor neurons except HE(18).

We performed a three-way ANOVA and found no difference in IPSC amplitude between peristaltic and synchronous coordination modes ($F = 0.58$, $df = 1$, $P = 0.45$), but IPSC amplitude was significantly different across motor neurons ($F = 2.54$, $df = 14$, $P = 1.9 \times 10^{-3}$) and across interneurons ($F = 10.60$, $df = 3$, $P = 1.2 \times 10^{-6}$). There was also a significant interaction of interneuron X motor neuron ($F = 3.62$, $df = 23$, $P = 1.4 \times 10^{-7}$). For the same data set, we also performed a three-way ANOVA for intersegmental conduction delay and found no difference between peristaltic and synchronous coordination modes ($F = 2.18$, $df = 1$, $P = 0.14$), but intersegmental conduction delay was significantly different across motor neurons ($F = 102.48$, $df = 14$, $P = 7.0 \times 10^{-103}$) and across interneurons ($F = 356.29$, $df = 3$, $P = 1.0 \times 10^{-96}$). There was also a significant interaction of interneuron X motor neuron ($F = 4.03$, $df = 20$, $P = 1.4 \times 10^{-7}$).

These motor neuron and interneuron effects for intersegmental conduction delay are trivial because of course the different interneurons are in different segmental positions and the different segmental motor neurons are different distances from interneurons and from one another. Because no coordination mode-related differences were found for either IPSC amplitude or intersegmental conduction delay, in most of the further analyses, data from the two coordination modes were combined.

Figure 2 illustrates how synaptic strength varies with premotor interneuron and segment and how conduction delay

varies with segment. The recordings show the spike-triggered average IPSCs elicited by an HN(4) and an HN(7) premotor interneuron in different preparations for a segmental series of ipsilateral motor neurons. Considering the HN(4) interneuron first, one sees that average IPSC amplitude increased and then decreased as the recordings progressed from front to rear motor neurons. Beyond segment 13 in this preparation, no spike-triggered IPSC was detected. Considering the HN(7) interneuron, one sees that average IPSC amplitude also increased and then decreased as the recordings progressed from front to rear motor neurons, but even in the rearmost motor neuron the average IPSC amplitude was easily detected.

Conduction delays progressed in 20- to 30-ms increments for both premotor interneurons from segment to segment for the first several segments but then progress seemed to stop or jump back. This lack of progression in the conduction delays may be artifactual and derive from the spike-triggered average technique. For most of the duration of their bursts, the premotor interneurons tended to fire at a quasi-constant rate, often resulting in multiple peaks in the spike-triggered average. We always chose the largest of these peaks as the average of directly elicited IPSCs (see METHODS). When the peaks were small, as they often were in rear motor neurons (especially when elicited by front premotor interneurons), there can be ambiguity. Moreover, accurate spike-triggered averages depend on constant conduction delays for each spike in a burst. We subsequently show that spike conduction delay varied during a burst. If conduction delay varies in a burst, then the temporal disparity of the individual IPSCs contributing to the average IPSC will increase with larger conduction distances (increased segment number between the presynaptic premotor interneuron and its postsynaptic motor neuron), leading to underestimates of average PSC amplitude and broad (potentially ambiguous) peaks in the spike-triggered average. Thus in Fig. 2 we suggest a peak (with a "?"), which is not the largest but may reflect the directly triggered IPSCs because it occurs at the predicted time based on regular progression of the conduction delay. These types of observations indicate that we probably underestimated synaptic strength in the rearmost motor neurons and that, by always choosing the largest peak in the spike-triggered average, we may have introduced errors in measurements of conduction delay when measurements span several segments. Nevertheless, because much of our data were taken from incomplete or short series of motor neurons, we were not able to infer potential corrections in many cases and therefore we chose the objectivity of the amplitude criterion.

Table 1 summarizes the data obtained for synaptic strength (IPSC amplitude) and conduction delays. Despite the sources of error cited earlier, these data show that the conduction delays averaged across preparations follow a segmental progression with moderate variability [coefficient of variation (CV), mostly in the range of 0.1–0.2]. The levels of variability (CV) across preparations in the average peak conductance of spike-triggered averaged IPSCs of at least the strong (average >1 nS) connections were in the range of 0.3–1.0. Especially for weak connections, we often observed no peak in the spike-triggered average and thus recorded a 0 value in the data of Table 1. These 0 values (the number of zero values are indicated for each connection in Table 1) can arise from two sources: a lack of a synaptic connection or measurement error. Given the problem of temporal dispersion in the spike-triggered average IPSC mentioned earlier we thus interpreted 0 values differently in front- and rearmost motor neurons. For example, the large number of 0 values for the connection from the HN(4) interneuron to the HE(4) motor neuron or the HN(7) interneuron to the HE(7) motor neuron probably reflects the absence of a functional synaptic contact because temporal dispersion should not be a problem within a ganglion, whereas the large number of 0 values for the connection from the HN(3) or HN(4) interneuron to the HE(16) or HE(17) motor neurons may represent a weak connection hard to detect due to the problems of temporal dispersion. Notwithstanding the origin of the 0 values, in determining an average of the ISPC amplitude across preparations (different animals) all 0 values were included in the average and are reflected in the large CV (>1) of weak connections (Table 1).

Figure 3*A* summarizes the average peak conductance of the IPSC of each identified premotor heart interneuron onto each segmental heart motor neuron across all 69 preparations used in these experiments. Error bars are omitted from the diagram for clarity; the SDs of average values plotted are given in Table 1. It represents a connectivity diagram and a synaptic strength diagram at the same time and shows clearly that the premotor interneurons vary in their synaptic strength from segment to segment so that different regions of segmental motor neurons are "dominated" by different sets of identified premotor interneurons; each has its own segmental profile of synaptic strength. For example, the HE(8) motor neuron received strong inhibitory synaptic input from all the identified premotor interneurons, whereas the HE(14) motor neuron received strong inhibitory synaptic input only from the rear [HN(6) and HN(7)] premotor interneurons. We subjected the IPSC amplitude data of Table 1 to a three-way ANOVA, which showed a significant effect for both the presynaptic heart interneuron [HN(3), HN(4), HN(6), HN(7)] ($F = 25.04$, $df = 3$, $P = 2.8 \times 10^{-15}$) and the postsynaptic heart motor neuron [HE(3)–HE(18)] ($F = 14.75$, $df = 15$, $P = 1.87 \times 10^{-32}$). There was also a significant interaction for the interneuron X motor neuron ($F = 6.11$, $df = 37$, $P = 9.6 \times 10^{-24}$). Because our aim was to measure synaptic strength of each identified premotor interneuron on every segmental motor neuron and not to show segmental differences statistically, pairwise tests were not pursued. We also computed a synaptic sum that is the sum of all the synaptic conductances on a given motor neuron. Under this analysis the middle motor neurons receive the heaviest inhibition, whereas the rearmost motor neurons receive very little inhibition (Table 1).

Figure 3*B* summarizes the average conduction delay of the IPSC of each identified premotor heart interneuron onto each segmental heart motor neuron across all 69 preparations used in these experiments. It shows that this segmental delay progresses regularly by 20–30 ms per segment for each identified premotor interneuron. Only at the very end of the nerve cord for the weak connections of the HN(3) and HN(4) interneurons does the progression break down as described earlier for Fig. 2. Error bars are omitted from the diagram for clarity; the SDs of average values plotted are given in Table 1.

To explore whether the segmental profile of synaptic strength suggested by the averaged data (Fig. 3*A*) for each identified premotor interneuron reflects real stereotypy, we plotted such profiles for each preparation where the series of motor neurons assessed for a particular interneuron was four or

TABLE 1. *Peak conductance (mean, SD, CV, n, zeros) and conduction delay (mean, SD, CV, n) for spike-mediated transmission in HE(3)–HE(18) heart motor neurons for all premotor HN interneurons*

		HE															
		3	4	5	6	7	8	9	10	11	12	13	14	15	16	17	18
HN(3)																	
Conductance, nS	Mean	12.8	10.1	6.9	5.6	5.1	6.7	5.0	3.8	2.8	2.1	1.6	1.0	0.8	0.3	0.6	0.7
	SD	6.6	5.6	5.8	3.8	3.0	3.6	3.0	2.0	1.4	1.6	1.4	1.3	1.7	0.8	1.1	1.1
	CV	0.5	0.6	0.8	0.7	0.6	0.5	0.6	0.5	0.5	0.8	0.8	1.3	2.0	2.6	1.9	1.5
	n	20	21	14	9	9	13	13	14	14	11	11	10	8	7	7	7
	Zeros	0	0	2	1	1	1	2	2	2	2	4	6	6	6	5	4
Delay, ms	Mean	6.3	29.2	61.1	91.6	131.4	140.0	155.0	177.6	205.1	238.7	279.4	263.1	333.0	330.6	389.2	354.9
	SD	1.2	3.2	8.4	15.1	13.8	27.8	29.9	28.7	31.5	42.5	44.7	18.2	5.5	0.0	47.4	30.9
	CV	0.2	0.1	0.1	0.2	0.1	0.2	0.2	0.2	0.2	0.2	0.2	0.1	0.0	0.0	0.1	0.1
	n	20	21	12	8	8	12	11	12	12	9	7	4	2	1	2	3
HN(4)																	
Conductance, nS	Mean		0.3	3.4	5.1	7.7	11.3	7.7	5.8	4.4	3.7	2.5	1.7	1.2	0.2	0.9	1.0
	SD		0.6	2.1	2.0	4.6	5.4	4.0	3.8	2.4	2.3	1.6	1.8	1.3	0.6	1.2	0.8
	CV		1.9	0.6	0.4	0.6	0.5	0.5	0.7	0.5	0.6	0.7	1.0	1.1	3.0	1.4	0.8
	n		13	12	13	11	12	20	19	17	12	10	9	10	9	9	8
	Zeros		6	0	0	0	0	1	2	2	2	2	4	4	8	5	3
Delay, ms	Mean		8.2	34.0	61.1	87.7	98.9	136.7	145.8	181.0	201.0	245.3	282.5	320.2	391.8	360.2	403.2
	SD		4.5	5.2	9.9	23.9	12.2	33.1	28.7	30.3	21.3	43.3	35.2	18.1	0.0	41.2	63.0
	CV		0.6	0.2	0.2	0.3	0.1	0.2	0.2	0.2	0.1	0.2	0.1	0.1	0.0	0.1	0.2
	n		8	12	13	11	12	19	17	15	10	8	5	6	1	4	5
HN(6)																	
Conductance, nS	Mean				1.2	4.8	7.6	7.9	7.7	7.1	5.3	4.5	6.2	3.5	3.6	2.0	2.1
	SD				1.4	2.7	3.8	3.6	1.9	3.0	3.1	2.2	1.4	1.7	1.2	1.7	0.8
	CV				1.2	0.6	0.5	0.5	0.3	0.4	0.6	0.5	0.2	0.5	0.3	0.9	0.4
	n				5	12	12	15	13	17	12	13	12	9	8	7	8
	Zeros				2	0	0	0	0	0	0	0	0	1	0	2	0
Delay, ms	Mean				4.3	38.4	65.6	97.1	128.2	162.9	195.3	206.9	228.0	254.4	266.3	294.1	320.6
	SD				2.2	6.3	8.1	16.3	20.6	22.6	26.5	25.6	21.9	30.5	23.2	40.5	27.8
	CV				0.5	0.2	0.1	0.2	0.2	0.1	0.1	0.1	0.1	0.1	0.1	0.1	0.1
	n				3	12	12	15	13	17	12	13	12	8	8	5	8
HN(7)																	
Conductance, nS	Mean					1.0	5.3	6.9	8.3	7.0	9.4	7.4	6.9	6.5	7.4	3.8	1.8
	SD					1.8	1.4	2.3	3.5	3.2	4.6	4.2	4.6	4.1	3.8	3.6	1.6
	CV					1.8	0.3	0.3	0.4	0.4	0.5	0.6	0.7	0.6	0.5	1.0	0.9
	n					4	14	18	21	16	14	13	9	12	9	8	8
	Zeros					2	0	0	0	0	0	1	1	2	1	2	2
Delay, ms	Mean					6.5	34.2	61.6	92.0	118.9	141.0	176.6	198.3	214.3	231.6	255.9	271.5
	SD					0.6	7.9	8.3	9.6	12.6	22.0	11.8	13.3	22.0	24.1	31.1	51.4
	CV					0.1	0.2	0.1	0.1	0.1	0.2	0.1	0.1	0.1	0.1	0.1	0.2
	n					2	14	18	21	16	14	12	8	10	8	6	6
HN(X) peri																	
Conductance, nS	Mean	8.4	7.8	5.3	2.2												
	SD	4.2	3.4	2.7	0.1												
	CV	0.5	0.4	0.5	0.0												
	n	7	5	3	2												
	Zeros	0	0	0	0												
HN(X) synch																	
Conductance, nS	Mean	5.7	4.6	3.2	1.8												
	SD	2.9	1.7	1.6	0.0												
	CV	0.5	0.4	0.5	0.0												
	n	7	5	3	2												
	Zeros	0	0	0	0												
Synaptic sum, nS		19.9	16.6	14.5	13.9	18.7	30.9	27.5	25.6	21.4	20.6	16.0	15.8	12.0	11.5	7.2	5.7

Values are means ± SD. CV = SD/mean. Zeros indicate the number of preparations where no IPSC was recorded for a particular HN interneuron in a particular HE motor neuron, although a measurable IPSC was recorded in other preparations. Data are combined for peristaltic and synchronous coordination modes except for the HN(X) interneuron. Synaptic sum is the total postsynaptic conductance of all the interneurons converging on that particular motor neuron. To construct this sum the peristaltic and synchronous HN(X) postsynaptic conductances on a given HE(3)–HE(6) motor neuron were averaged. See METHODS.

greater (Fig. 4). Particularly for the HN(3) and HN(4) interneurons the individual preparations displayed the same general segmental profile: strong to weak for the HN(3) interneuron and weak to strong to weak for the HN(4) interneuron. For the HN(6) and HN(7) interneurons, the profiles of the individual preparations were more erratic but they generally conveyed near equality of strength across a broad range of segmental motor neurons with reduced strength at the ends of the range. Supplemental Fig. 1[1] shows the complete range of synaptic strength for each identified premotor interneuron motor neuron

[1] The online version of this article contains supplemental data.

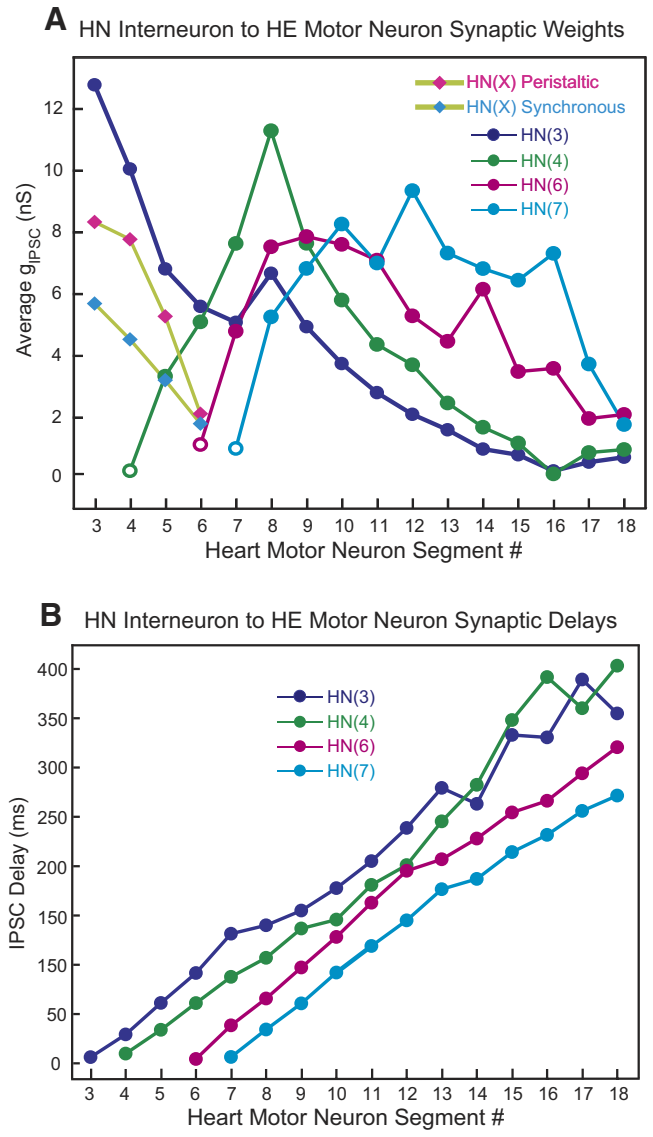

FIG. 3. Heart interneuron to heart motor neuron inhibitory synaptic strengths: segmental profile (*A*) and conduction delays (*B*). *A*: synaptic strengths are indicated as conductances [in nanosiemens (nS)] and spike-triggered averages from several preparations were averaged to produce the value for each segmental heart motor neuron. See Table 1 for numerical values: means, SDs, coefficient of variation, number of zeros, and number of observations. Unfilled circles indicate average strengths for segmental motor neurons where the corresponding interneuron—in the ganglion of origin of the interneuron—only occasionally makes a synaptic connection. *B*: conduction delays measured as the delay to the peak of spike-triggered average IPSCs in successive segmental heart motor neurons averaged across preparations are similar for each identified premotor heart interneuron and progress regularly by 20–30 ms per segment. Note that the monotonic progression becomes irregular for the weak connections from the HN(3) and HN(4) premotor interneurons to the rear motor neurons. See Table 1 for numerical values: means, SDs, coefficient of variation, and number of observations.

pair recorded in the 69 preparations used in these experiments. There are remarkably few apparent outliers in our data set, giving us confidence that the variability seen is mostly biological and not experimental error. The zeros in the data set, particularly for connections that in the majority of preparations show a large conductance, represent potential experimental errors; the number of zeros for each connection is given in Table 1.

Synaptic plasticity of identified premotor interneurons

The same recordings used earlier for the analysis of synaptic strength and conduction delay all displayed synaptic plasticity of the identified premotor interneuron to motor neuron inhibitory synaptic connections. It has long been known that the size of spike-mediated inhibitory synaptic potentials from heart interneurons onto their postsynaptic targets varies during a burst, increasing and then decreasing in size, and that spike-mediated IPSP size is sensitive to the baseline membrane potential from which the spike arises (Nicholls and Wallace 1978; Olsen and Calabrese 1996; Thompson and Stent 1976; Tobin and Calabrese 2005) and ultimately due to background Ca^{2+} dynamics controlled by low-threshold Ca^{2+} currents and not spike frequency (Ivanov and Calabrese 2003). Nevertheless this short-term plasticity has not been systematically explored under the normal operating condition of the heartbeat central pattern generator during fictive heartbeat.

We analyzed data from 11 preparations each with two premotor interneurons recorded (covering all identified premotor interneurons and a variety of segmental heart motor neurons) to compare synaptic plasticity between coordination modes of each identified premotor interneuron. We used 10–20 bursts of presynaptic spikes in both coordination modes and made spike-triggered averages for each numerically sequential spike in the bursts. This procedure allowed us to determine synaptic plasticity (i.e., how synaptic strength varied during a presynaptic burst) across identified premotor interneurons and motor neurons. It also allowed us to assess whether conduction delay varied during a burst. Figure 5 shows typical records from a preparation used in this analysis, illustrating two premotor interneurons converging onto the same motor neuron.

The same general pattern was seen in both coordination modes and for both presynaptic premotor interneurons, although of course the average synaptic strength and conduction delay varied between the two premotor interneurons. Early spikes (e.g., spikes 1–5) led to very small IPSCs, spikes in the middle of the bursts (e.g., spikes 10–20) led to large IPSCs, and spikes at the end of the bursts (e.g., spikes ≥30) again led to small IPSCs but not as small as at the beginning of the bursts. Conduction delays became increasingly longer during the burst. We have previously shown for the heart motor neurons, using two point recordings, that spike conduction in peripheral nerves becomes increasingly slower during a burst (Wenning et al. 2004b), and we hypothesized that a similar slowing of axonal conduction of action potentials was occurring in the premotor heart interneurons. The similarity of synaptic plasticity between synchronous and peristaltic coordination modes allowed us to combine records from the two modes and thus increase spike numbers for our averages; this was particularly advantageous when exploring plasticity of weak distant connections to the rearmost heart motor neurons.

In eight preparations (different from those in the preceding paragraph), we recorded 10 premotor interneurons (covering all the identified premotor interneurons), each with long series of segmental heart motor neurons, and assessed synaptic plasticity combining data from synchronous and peristaltic bursts. Analyses of recordings from two such preparations, shown in Fig. 6, are typical and indicate that the general pattern of synaptic plasticity, described earlier, holds for both interneurons and for all of their synaptic inputs to motor neurons.

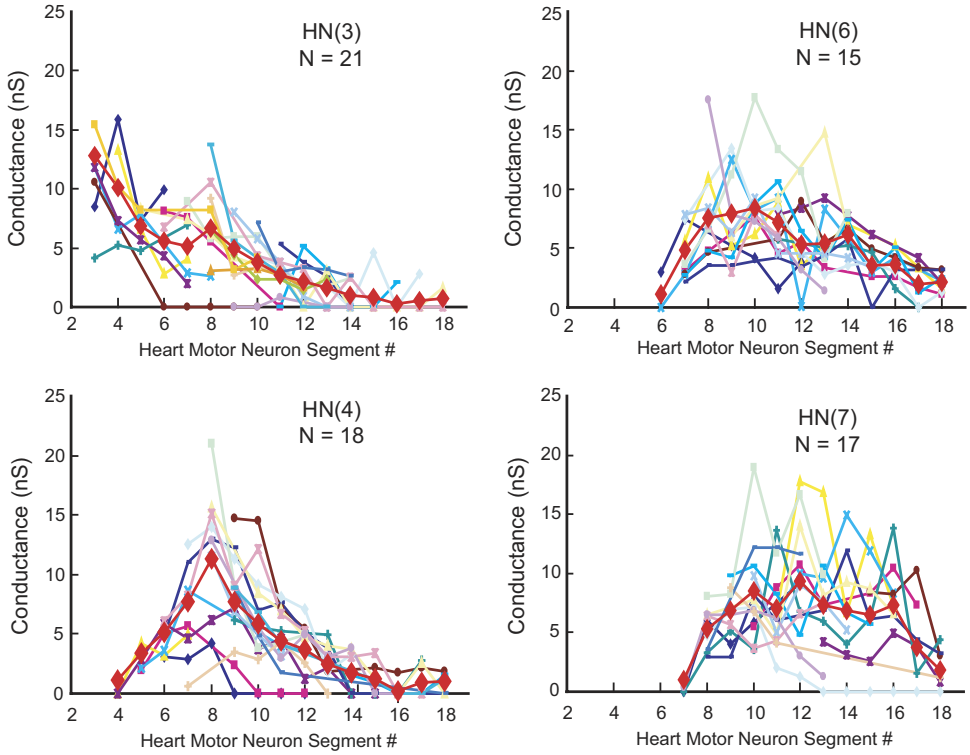

FIG. 4. Animal-to-animal variability in the segmental profile of synaptic strength of identified premotor interneurons. Conductances of spike-triggered average IPSCs in a segmental series of ≥4 heart motor neurons produced by an ipsilateral premotor interneuron in different preparations (individual animals) are plotted separately. Each panel shows the segmental profile of synaptic strength in *n* individual animals (a different color is used for each preparation) for a different identified premotor interneuron. Average synaptic strengths for each interneuron from Fig. 3*A* are plotted with large red diamonds.

Connectivity, synaptic strength, and synaptic plasticity of the unidentified HN(X) premotor interneuron

We indirectly measured the activity of the unidentified HN(X) interneurons by recording their synaptic currents in known postsynaptic targets. The HN(X) interneurons are defined by their input to HE(3)–HE(6) motor neurons on both peristaltic and synchronous sides, and their electrical coupling to ipsilateral HN(3) and HN(4) heart interneurons (Fig. 1*A*) (Calabrese 1977; Norris et al. 2006). These HN(X)-mediated IPSCs are strong in the HE(3) and HE(4) motor neurons and get weaker in the HE(5) and HE(6) motor neurons. Similarly to the method described in Norris et al. (2006), by recording the HN(3) and HN(4) interneuron and ipsilateral HE(3)–HE(6) motor neurons one can unambiguously assign all IPSCs mediated by the HN(3) and HN(4) interneurons and thus by "subtraction" determine the IPSCs mediated by the HN(X) interneuron and thus its firing pattern and synaptic strength. This method is illustrated in Fig. 7. We used 13 preparations in this analysis. In nine preparations both the HN(3) and the HN(4) interneurons were recorded, so HN(X)-mediated IPSC could be identified and assessed in all four of the HN(X) interneuron postsynaptic targets [HE(3)–HE(6) motor neurons]. In the other four preparations, only the HN(3) interneuron was recorded so identification of HN(X)-mediated IPSCs and thus analysis was limited to the HE(3) and HE(4) motor neurons (Fig. 1*A*).

The HN(X)-mediated IPSCs are very small in the HE(5) and especially the HE(6) motor neurons, and so they were difficult to detect, restricting both the number of recordings that were successful and our ability to detect all the HN(X)-mediated

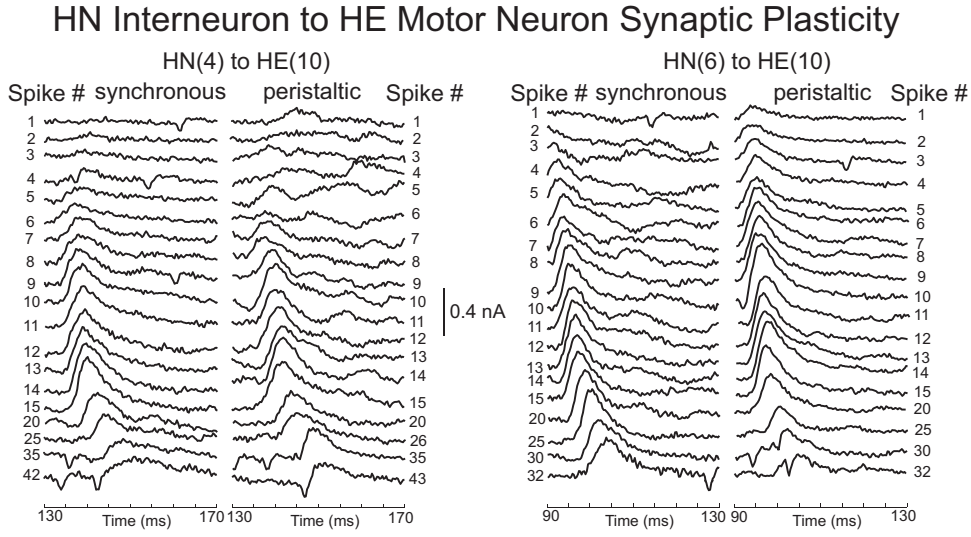

FIG. 5. Spike-triggered averages of IPSCs for sequential spikes in premotor heart interneuron bursts to illustrate synaptic dynamics of the heart interneuron to heart motor neuron connections. Total of 15 bursts in each coordination mode of an HN(4) and an HN(6) interneuron were divided into sequential spikes 1 to >30 and spike-triggered averages of IPSCs were computed from voltage-clamp recordings of an ipsilateral HE(10) motor neuron. Average IPSCs for the first 15 spikes are shown and then for a selection of subsequent spikes (IPSC #). For some spikes near the end of a burst, <15 bursts had such spikes, so less triggering spikes were used to compute the average: IPSC 43 for HN(4) to HE(10) peristaltic: 14 spikes; IPSCs 30 and 32 for HN(6) to HE(10) synchronous: 14 and 10 spikes, respectively; IPSCs 30 and 32 for HN(6) to HE(10) peristaltic: 12 and 10 spikes, respectively. Timescale origin is the time of the triggering spike event. All records made simultaneously from the same preparation.

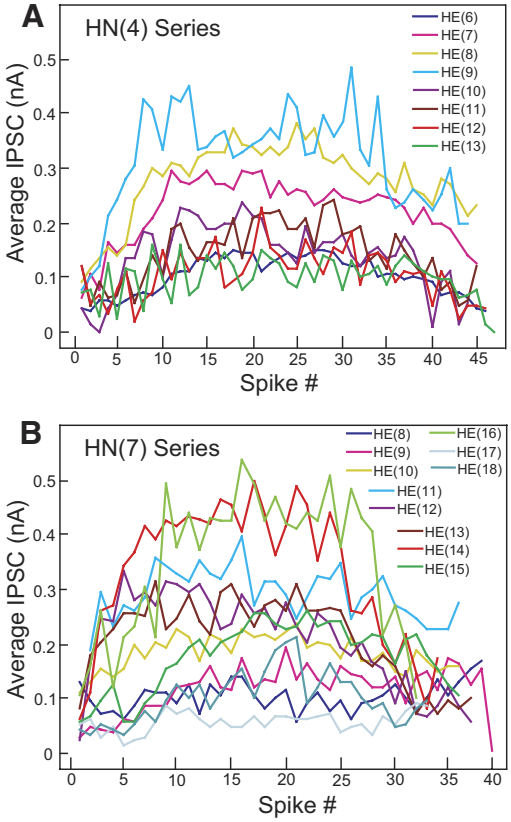

FIG. 6. Synaptic dynamics in an ipsilateral segmental series of heart motor neurons for 2 different premotor heart interneurons. Average IPSC peak amplitude [in nanoamperes (nA)] for sequential spikes in 15 premotor interneuron bursts computed as in Fig. 5; for some spikes near the end of a burst, <15 bursts had such spikes, so less triggering spikes were used to compute the average. Different motor neurons indicated with different symbols and colors according to graph key. *A*: HN(4) interneuron synaptic series. All recordings are from the same preparation. *B*: HN(7) interneuron synaptic series. All recordings are from the same preparation.

IPSCs in a "burst." As can be see in Fig. 7, fewer HN(X)-mediated IPSCs could be detected in the HE(5) motor neuron than in the HE(3) motor neuron in both coordination modes, but those detected in the HE(5) motor neuron matched one for one with those detected in the HE(3) motor neuron. The small size of HN(X)-mediated IPSCs in the HE(5) and HE(6) motor neurons thus appears to compromise our detection; nevertheless those detected probably reflect the amplitude of the population. As described in Norris et al. (2006), the HN(X) interneuron has very different firing characteristics in the two coordination modes; there are fewer HN(X)-mediated IPSCs and they occur at lower frequency in the peristaltic mode than in the synchronous mode. These differences and a visually apparent difference in the amplitude of IPSCs in the two coordination modes in the HE(3) and HE(4) motor neurons caused us to analyze data from the two coordination modes separately.

Keeping data from the different coordination modes separate, we averaged the peak conductance of the IPSCs in 0.05-phase bins during the burst cycle of the ipsilateral HN(4) interneuron (phase marker neuron) across the different preparations, usually with 11–13 IPSC bursts per coordination mode in each motor neuron recorded (see METHODS). The HN(4) phase-marker interneuron was assigned a phase of 0.0 during peristaltic coordination and 0.511 during synchronous coordinations as described in Norris et al. (2006). When the ipsilateral HN(4) interneuron was not recorded the ipsilateral HN(3) interneuron was used as a phase marker and phase was adjusted by 0.026 (peristaltic mode) and 0.045 (synchronous mode), which represent the average phase lead of an HN(4) interneuron over its ipsilateral HN(3) interneuron (Norris et al. 2006). These measurements reflect IPSCs elicited only during the middle of the HN(X) interneuron burst because our procedure will have missed small HN(X)-mediated IPSCs that occur at the beginning and end of the IPSC burst, especially in the HE(5) and HE(6) motor neurons where even the largest IPSCs are small. Moreover, large IPSCs mediated by the HN(3) and HN(4) interneurons in these motor neurons can obscure the HN(X)-mediated IPSCs. Results of this analysis are illustrated in Fig. 8 and show that the strength (peak conductance) of the HN(X)-mediated IPSCs declines dramatically from the HE(3) to the HE(6) motor neuron in both coordination modes. This analysis also indicates that HN(X)-mediated IPSC peak conductance varies across the HN(X) interneuron burst similarly to the synaptic plasticity expressed at the connections of the identified premotor interneurons (Fig. 5).

To summarize the data of Fig. 8 and to make them comparable to the averaged IPSCs from individual spike-triggered averages mediated by the identified premotor interneurons (Table 1, Fig. 3*A*), we averaged conductance across the phase bins for the HN(X)-mediated IPSC in each of the motor neurons [HE(3)–HE(6)], but still keeping the coordination modes separate. To test for differences in these averaged peak conductances between the coordination modes, we sought a simplified approach because our limited data set for the HE(5) and HE(6) motor neurons precluded a meaningful three-way ANOVA. Therefore we did not perform multiple comparisons but performed paired *t*-tests instead for the HE(3) and HE(4) motor neurons across coordination mode for HN(X)-mediated IPSC peak conductance and showed that for both motor neurons the peristaltic peak conductance was significantly greater than the synchronous peak conductance ($t = 3.78$, $df = 6$, $P = 9.2 \times 10^{-3}$ and $t = 4.20$, $df = 4$, $P = 1.4 \times 10^{-2}$, respectively). Thus we felt justified in keeping data for the two coordination modes separate for HN(X)-mediated IPSCs. These averaged data are summarized in Table 1 and Fig. 3*A*.

Graded synaptic transmission in motor neurons receiving input from the HN(X) premotor interneuron

In the same recordings described in the previous section (13 preparations and using the same bursts used to analyze spike-mediated IPSCs), we estimated a putative graded component of transmission onto the HE(3) to HE(6) motor neurons by filtering out the fast IPSCs and any escaping spike currents, thus generating a slow current wave of motor neuron synaptic input. These slow waves are illustrated in Fig. 7 for the HE(3) and HE(5) motor neurons in peristaltic (pink curve) and synchronous (light blue curve) coordination mode. We converted these slow current waves to conductance, averaging the slow-wave cycles for each cell in each coordination mode. We measured the peak amplitude for each average wave and the results of this analysis are shown in Table 2. The variability among preparations makes generalization difficult, although some trends may be discerned. The HE(3) and HE(4) motor neurons

can show very strong graded transmission in both the peristaltic and synchronous coordination modes compared with that observed in other motor neurons that do not receive HN(X) input (cf. Figs. 1 and 7). This observation suggests that such strong graded transmission is associated with activity in the HN(X) interneuron (see also Table 1). The graded transmission in the HE(5) and HE(6) motor neurons is less strong. It is unclear at this point whether these slow waves represent graded transmission or the summated slow components of the postsynaptic current elicited by HN(X) spikes.

DISCUSSION

Here we systematically measured the strength and dynamics of the synaptic connections and the associated conduction delays from premotor interneurons to segmental motor neurons for the heartbeat CPG of the leech. We explored whether these connections changed in the two coordination modes that reflect alternative outputs of the heartbeat CPG and concluded that they did not. We also considered how the strength of these connections varied across preparations and concluded that there is a stereotypical pattern of intersegmental connectivity despite wide variations among preparations. To extract insights from this analysis we address three questions.

Is the segmental profile synaptic strength of each of the identified premotor heart interneurons stereotypical across animals?

There is growing recognition that critical parameters for network function, the values of maximal conductances of various intrinsic membrane currents and of synaptic connections, vary from individual to individual and that several different parameter sets may lead to similar network function (Marder and Goaillard 2006; Prinz et al. 2004; Schulz et al. 2006; although for a contrary view see Nowotny et al. 2007; Szucs and Selverston 2006). That the diversity seen is the result of activity-dependent homeostatic tuning for proper neuron and network function is now actively discussed. These ideas can lead to the conclusion that it is hopeless to attempt what we have attempted here, that is, to describe the pattern of synaptic strength in a network—specifically here in the connections between the premotor interneurons of a CPG and the ensemble of segmental motor neurons it controls—because many synaptic strength patterns can lead to the same outcome. The patterns that we have observed here indicate that average measurements define the tendency that a particular connection will be strong or weak. For example, we never observed a strong connection from the HN(4) interneuron to the HE(15) motor neuron but the connection of the HN(7) interneuron to the same HE(15) motor neuron was almost always strong and the connections of the HN(4) interneuron and the HN(7) interneuron to the HE(8) motor neuron were usually strong,

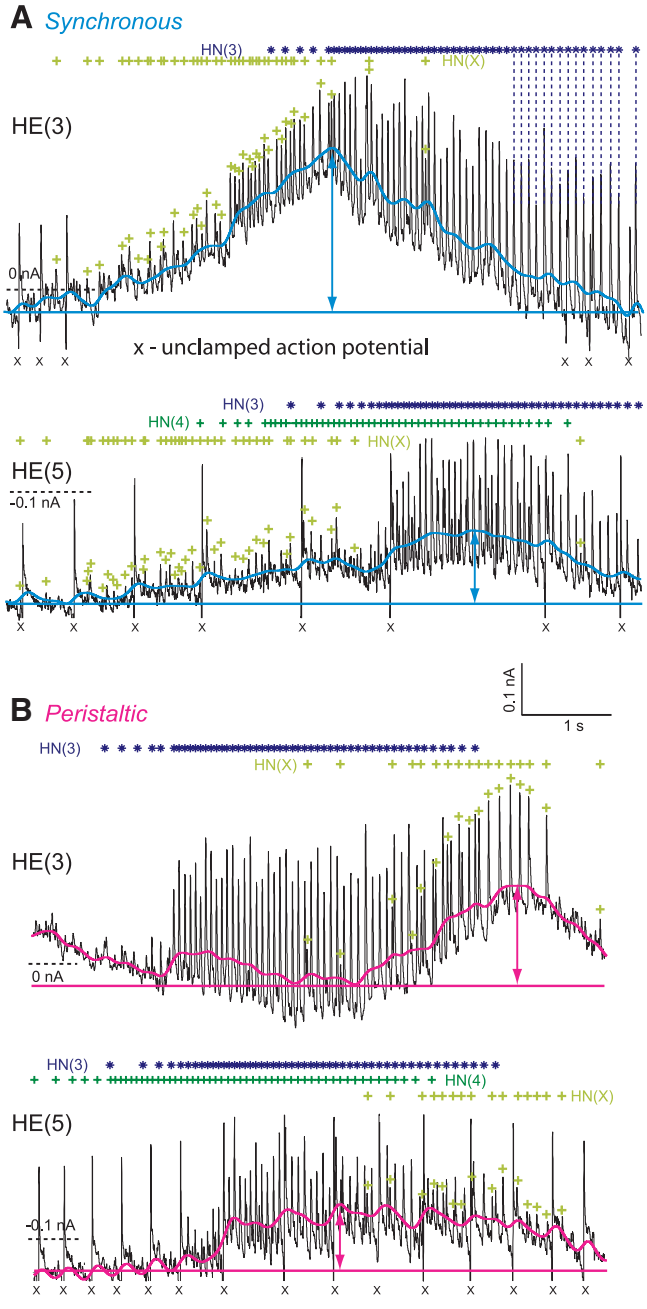

FIG. 7. Detecting HN(X)-mediated IPSCs in ipsilateral HE(3) and HE(5) heart motor neurons to measure the IPSC peak amplitude and total graded transmission. Bursts of IPSCs recorded under voltage clamp in an HE(3) and an HE(5) motor neuron in the synchronous (light blue, *A*) and peristaltic (pink, *B*) coordination mode from the same preparation. Spike activity was recorded extracellularly in ipsilateral HN(3) and HN(4) interneurons. Spikes of the ipsilateral HN(3) interneuron are indicated by dark blue asterisks above each current trace and were used to identify HN(3)-mediated IPSCs in the HE(3) and HE(5) motor neurons [vertical dashed lines indicate some of the identified HN(3)-mediated IPSCs in the HE(3) motor neuron]. Spikes of the ipsilateral HN(4) interneuron are indicated by dark green asterisks above each current trace and were used to identify HN(4)-mediated IPSCs in the HE(5) motor neuron. Remaining unidentified IPSCs (meeting criteria outlined in METHODS) were ascribed to the ipsilateral HN(X) interneuron (lime green cross marker). Note the different ipsilateral phase of the HN(X)-mediated IPSCs with respect to the ipsilateral HN(4) interneuron's burst (phase reference) in the 2 coordination modes. IPSC peak amplitude was measured from baseline just before the IPSC. Filtered waveform of the graded IPSC (synchronous, wavy light blue line; peristaltic, wavy pink line) and baseline outward current (horizontal colored lines) used to measure graded transmission are also indicated on each record (see METHODS). Peak graded transmission amplitude is indicated for each waveform by a vertical double-headed arrow. Similar results were obtained in other preparations as indicated by average data in Fig. 8 (spike-mediated IPSCs) and Table 2 (graded PSCs). Note that there are more HN(X)-mediated IPSCs in the synchronous than in the peristaltic coordination mode, and that HN(X)-mediated IPSC frequency accelerates during a "burst" in the synchronous mode.

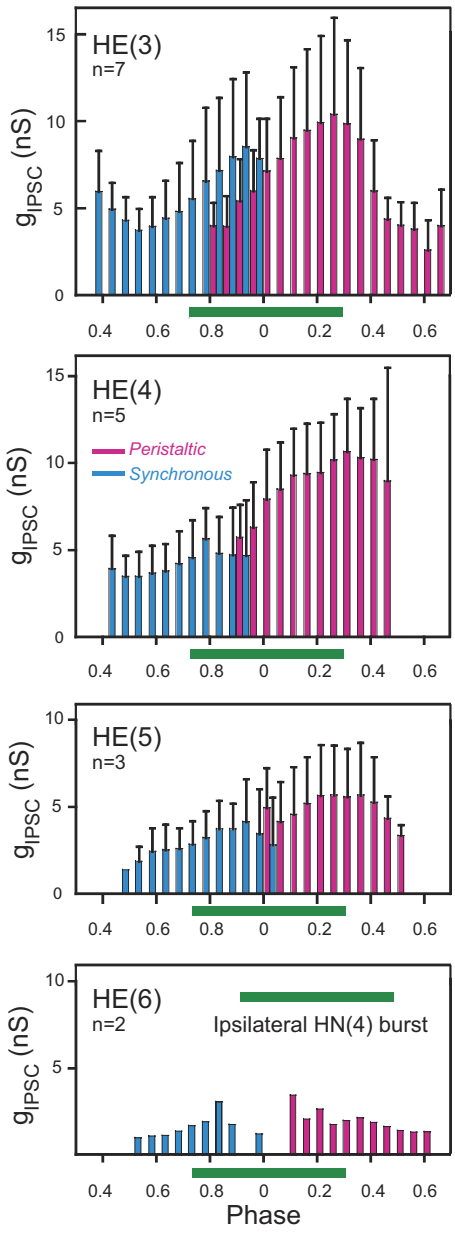

FIG. 8. Graphic illustration of the synaptic strength and dynamics of HN(X)-spike-mediated IPSCs in HE(3)–HE(6) motor neurons in peristaltic (pink) and synchronous (light blue) coordination mode. Activity cycle of the HN(4) heart interneuron phase reference was divided into 0.05-phase bins and the mean amplitude [±SD, except for the HE(6) motor neuron, where the values averaged were peristaltic: 2.19 and 2.12 nS, and synchronous: 1.81 and 1.85 nS] of the HN(X)-spike-mediated IPSCs in heart motor neurons in each phase bin was plotted for the number of preparations indicated on each panel for a particular motor neuron HE(3)– HE(6). HN(X)-spike-mediated IPSCs were identified and measured as indicated in Fig. 7; see METHODS for further details. Green bar: duty cycle of the ipsilateral HN(4) premotor interneuron with the middle spike at 0.0 phase.

although on average stronger for the HN(4) interneuron (Figs. 2 and 4). Minimally then, for comparisons between different cells in a network, average data can indicate trends and by defining the physiological range can set useful limits on parameters.

Figure 4, in particular, indicates that the segmental profiles of connection strength of premotor interneurons seen in average data are observed in individual preparations. An attractive hypothesis is that average data for premotor heart interneurons in fact show the relative strengths of all synapses within and between presynaptic neurons in the network and that the physiological range is simply a constant multiplicative adjustment of these relative strengths, i.e., the segmental profiles of premotor interneuron synaptic connections are stereotypical. Proving this hypothesis statistically will require more extensive data sets from individual preparations than we have been able to accomplish in our experiments.

What is different about CPG synaptic output in the peristaltic and the synchronous coordination modes?

We have argued here that for the identified premotor interneurons of the heart CPG there are no differences in the strength and dynamics of their synaptic output onto segmental motor neurons in the peristaltic and synchronous coordination modes (Figs. 2 and 4). No statistical differences were found for synaptic strength and, although synaptic dynamics in the two modes were compared statistically, no substantive differences could be discerned in our data. Moreover, our previous analysis of the activity pattern of the identified premotor interneurons noted no substantive (statistically significant) differences in burst duration or average spike frequency of corresponding identified premotor interneurons in peristaltic and synchronous coordination modes (Norris et al. 2006). Thus with respect to the identified premotor interneurons, only their intersegmental phase relations differ in peristaltic and synchronous coordination.

The situation is quite different when considering the unidentified HN(X) interneuron. Not only do its phase relations with respect to the other premotor interneurons differ during peristaltic and synchronous coordination but so does its burst duration and average spike frequency (Fig. 7) (Norris et al. 2006) and as shown here its average synaptic strength (Fig. 8). Moreover the motor neurons that receive HN(X) input may also receive considerable graded synaptic inhibition (Fig. 7; Table 2), particularly in the HE(3) and HE(4) motor neurons. This graded inhibition in HE(3)–HE(6) motor neurons may be largely mediated by the HN(X) interneuron, which because of its strong spike-mediated (Fig. 8) and graded inhibitory input likely plays a major role in determining the activity pattern (particularly burst phase) of these motor neurons. Recordings such as those in Fig. 10 of the companion paper (Norris et al. 2007), where the activity phase of the HE(3) and HE(4) motor neurons shift with respect to the identified front premotor interneurons on a switch in coordination mode, further suggest an important role for the HN(X) interneuron in coordination of

TABLE 2. *Peak conductance for graded transmission in HE(3)–HE(6) heart motor neurons*

	Peak Conductance, nS		
Motor Neuron	Peristaltic	Synchronous	*n*
HE(3)	11.5 ± 6.4	14.6 ± 9.2	7
HE(4)	14.8 ± 3.0	7.5 ± 3.5	5
HE(5)	11.5 ± 6.6	7.4 ± 2.6	3
HE(6)	8.2	9.1	2

Values are means ± SD, except for HE(6), where the values averaged were peristaltic: 8.25 and 8.57 nS; and synchronous: 8.07 and 9.59 nS. See METHODS.

the HE(3)–HE(6) motor neurons. Moreover, the summary joint phase diagram of Fig. 12 of the companion paper (Norris et al. 2007) suggests that in the peristaltic mode the HN(X)-mediated inhibition (graded and spike-mediated) dominates the phasing of the HE(3)–HE(5) motor neurons, whereas in synchronous coordination mode the phasing of these motor neurons is dominated by HN(3)- and HN(4)-mediated inhibition.

Can the output of the central pattern generator be translated into the fictive motor pattern?

Our ultimate goal is to translate the fictive output of the heartbeat central pattern generator into the fictive heartbeat motor pattern. We reasoned that it would be important to measure as rigorously as possible the strength and dynamics, and associated conduction delays, of all the synaptic outputs of the CPG onto segmental heart motor neurons. These data and the previous quantitative analysis of the activity pattern of all the known premotor interneurons of the CPG (Norris et al. 2006), constrained by the quantitative description of the relative phasing of the CPG activity and the fictive motor program (activity in the ensemble of heart motor neurons) in the companion paper (Norris et al. 2007), will enable a first-generation model of how the CPG sculpts out the fictive heartbeat motor pattern by providing rhythmic inhibition to segmental motor neurons. With such a model we hope to be able to provide more mechanistic insights into this process.

ACKNOWLEDGMENTS

Present address of A. L. Weaver: Xavier University of Louisiana, Department of Biology, New Orleans, LA 70125.

GRANTS

This work was supported by the National Institute of General Medical Sciences National Research Service Award Institutional Research and Academic Career Development postdoctoral fellowship GM-000680 to A. L. Weaver and by National Institute of Neurological Disorders and Stroke Grant NS-24072 to R. L. Calabrese.

REFERENCES

Angstadt JD, Calabrese RL. Calcium currents and graded synaptic transmission between heart interneurons of the leech. *J Neurosci* 11: 746–759, 1991.

Burrows M. Co-ordinating interneurones of the locust which convey two patterns of motor commands: their connexions with flight motoneurones. *J Exp Biol* 63: 713–733, 1975a.

Burrows M. Co-ordinating interneurones of the locust which convey two patterns of motor commands: their connexions with ventilatory motoneurones. *J Exp Biol* 63: 735–753, 1975b.

Burrows M. Monosynaptic connexions between wing stretch receptors and flight motoneurones of the locust. *J Exp Biol* 62: 189–219, 1975c.

Burrows M, Pfluger HJ. Output connections of a wind sensitive interneurone with motor neurones innervating flight steering muscles in the locust. *J Comp Physiol A Sens Neural Behav Physiol* 171: 437–446, 1992.

Butera RJ Jr, Rinzel J, Smith JC. Models of respiratory rhythm generation in the pre-Bötzinger complex. I. Bursting pacemaker neurons. *J Neurophysiol* 82: 382–397, 1999a.

Butera RJ Jr, Rinzel J, Smith JC. Models of respiratory rhythm generation in the pre-Bötzinger complex. II. Populations of coupled pacemaker neurons. *J Neurophysiol* 82: 398–415, 1999b.

Calabrese RL. The neural control of alternate heartbeat coordination states in the leech, *Hirudo medicinalis. J Comp Physiol* 122: 111–143, 1977.

Cropper EC, Evans CG, Hurwitz I, Jing J, Proekt A, Romero A, Rosen SC. Feeding neural networks in the mollusc Aplysia. *Neurosignals* 13: 70–86, 2004.

Deliagina TG, Zelenin PV, Orlovsky GN. Encoding and decoding of reticulospinal commands. *Brain Res Brain Res Rev* 40: 166–177, 2002.

Del Negro CA, Johnson SM, Butera RJ, Smith JC. Models of respiratory rhythm generation in the pre-Bötzinger complex. III. Experimental tests of model predictions. *J Neurophysiol* 86: 59–74, 2001.

De Schutter E, Ekeberg O, Kotaleski JH, Achard P, Lansner A. Biophysically detailed modelling of microcircuits and beyond. *Trends Neurosci* 28: 562–569, 2005.

Golowasch J, Goldman MS, Abbott LF, Marder E. Failure of averaging in the construction of a conductance-based neuron model. *J Neurophysiol* 87: 1129–1131, 2002.

Haedo RJ, Golowasch J. Ionic mechanism underlying recovery of rhythmic activity in adult isolated neurons. *J Neurophysiol* 96: 1860–1876, 2006.

Hill AA, Masino MA, Calabrese RL. Intersegmental coordination of rhythmic motor patterns. *J Neurophysiol* 90: 531–538, 2003.

Hurwitz I, Susswein AJ. B64, a newly identified central pattern generator element producing a phase switch from protraction to retraction in buccal motor programs of *Aplysia californica*. *J Neurophysiol* 75: 1327–1344, 1996.

Ivanov AI, Calabrese RL. Modulation of spike-mediated synaptic transmission by presynaptic background Ca^{2+} in leech heart interneurons. *J Neurosci* 23: 1206–1218, 2003.

Ivanov AI, Calabrese RL. Graded inhibitory synaptic transmission between leech interneurons: assessing the roles of two kinetically distinct low-threshold Ca currents. *J Neurophysiol* 96: 218–234, 2006a.

Ivanov AI, Calabrese RL. Spike-mediated and graded inhibitory synaptic transmission between leech interneurons: evidence for shared release sites. *J Neurophysiol* 96: 235–251, 2006b.

Kotaleski JH, Grillner S, Lansner A. Neural mechanisms potentially contributing to the intersegmental phase lag in lamprey. I. Segmental oscillations dependent on reciprocal inhibition. *Biol Cybern* 81: 317–330, 1999a.

Kotaleski JH, Lansner A, Grillner S. Neural mechanisms potentially contributing to the intersegmental phase lag in lamprey. II. Hemisegmental oscillations produced by mutually coupled excitatory neurons. *Biol Cybern* 81: 299–315, 1999b.

Kristan WB Jr, Calabrese RL, Friesen WO. Neuronal control of leech behavior. *Prog Neurobiol* 76: 279–327, 2005.

Kristan WB Jr, Lockery SR, Lewis JE. Using reflexive behaviors of the medicinal leech to study information processing. *J Neurobiol* 27: 380–389, 1995.

Lockery SR, Kristan WB Jr. Distributed processing of sensory information in the leech. I. Input-output relations of the local bending reflex. *J Neurosci* 10: 1811–1815, 1990a.

Lockery SR, Kristan WB Jr. Distributed processing of sensory information in the leech. II. Identification of interneurons contributing to the local bending reflex. *J Neurosci* 10: 1816–1829, 1990b.

Lu J, Dalton JFt, Stokes DR, Calabrese RL. Functional role of Ca^{2+} currents in graded and spike-mediated synaptic transmission between leech heart interneurons. *J Neurophysiol* 77: 1779–1794, 1997.

Mamiya A, Nadim F. Target-specific short-term dynamics are important for the function of synapses in an oscillatory neural network. *J Neurophysiol* 94: 2590–2602, 2005.

Marder E, Bucher D. Understanding circuit dynamics using the stomatogastric nervous system of lobsters and crabs. *Annu Rev Physiol* 69: 291–316, 2007.

Marder E, Bucher D, Schulz DJ, Taylor AL. Invertebrate central pattern generation moves along. *Curr Biol* 15: R685–R699, 2005.

Marder E, Calabrese RL. Principles of rhythmic motor pattern generation. *Physiol Rev* 76: 687–717, 1996.

Marder E, Goaillard JM. Variability, compensation and homeostasis in neuron and network function. *Nat Rev Neurosci* 7: 563–574, 2006.

Nicholls J, Wallace BG. Modulation of transmission at an inhibitory synapse in the central nervous system of the leech. *J Physiol* 281: 157–170, 1978.

Norris BJ, Weaver AL, Morris LG, Wenning A, García PA, Calabrese RL. A central pattern generator producing alternative outputs: temporal pattern of premotor activity. *J Neurophysiol* 96: 309–326, 2006.

Norris BJ, Weaver AL, Wenning A, Garciá PA, Calabrese RL. A central pattern generator producing alternative outputs: phase relations of leech heart motor neurons with respect to premotor synaptic input. 98: 2983–2991, 2007.

Nowotny T, Szucs A, Levi R, Selverston AI. Models wagging the dog: are circuits constructed with disparate parameters? *Neural Comput* 19: 1985–2003, 2007.

Olsen OH, Calabrese RL. Activation of intrinsic and synaptic currents in leech heart interneurons by realistic waveforms. *J Neurosci* 16: 4958–4970, 1996.

Opdyke CA, Calabrese RL. Outward currents in heart motor neurons of the medicinal leech. *J Neurophysiol* 74: 2524–2537, 1995.

Pfluger HJ, Burrows M. Synaptic connections of different strength between wind-sensitive hairs and an identified projection interneuron in the locust. *Eur J Neurosci* 2: 1040–1050, 1990.

Prinz AA, Bucher D, Marder E. Similar network activity from disparate circuit parameters. *Nat Neurosci* 7: 1345–1352, 2004.

Rabbah P, Nadim F. Synaptic dynamics do not determine proper phase of activity in a central pattern generator. *J Neurosci* 25: 11269–11278, 2005.

Rybak IA, Shevtsova NA, Paton JF, Dick TE, St-John WM, Morschel M, Dutschmann M. Modeling the ponto-medullary respiratory network. *Respir Physiol Neurobiol* 143: 307–319, 2004a.

Rybak IA, Shevtsova NA, Paton JF, Pierrefiche O, St-John WM, Haji A. Modelling respiratory rhythmogenesis: focus on phase switching mechanisms. *Adv Exp Med Biol* 551: 189–194, 2004b.

Sautois B, Soffe SR, Li WC, Roberts A. Role of type-specific neuron properties in a spinal cord motor network. *J Comput Neurosci* 23: 59–77, 2007.

Schulz DJ, Goaillard JM, Marder E. Variable channel expression in identified single and electrically coupled neurons in different animals. *Nat Neurosci* 9: 356–362, 2006.

Siddall ME, Trontelj P, Utevsky SY, Nkamany M, Macdonald KS. Diverse molecular data demonstrate that commercially available medicinal leeches are not *Hirudo medicinalis*. *Proc Biol Sci* 274: 1481–1487, 2007.

Szucs A, Selverston AI. Consistent dynamics suggests tight regulation of biophysical parameters in a small network of bursting neurons. *J Neurobiol* 66: 1584–1601, 2006.

Thompson WJ, Stent GS. Neuronal control of heartbeat in the medicinal leech. III. Synaptic relations of the heart interneurons. *J Comp Physiol* 111: 309–333, 1976.

Tobin AE, Calabrese RL. Myomodulin increases I_h and inhibits the NA/K pump to modulate bursting in leech heart interneurons. *J Neurophysiol* 94: 3938–3950, 2005.

Tunstall MJ, Roberts A, Soffe SR. Modelling inter-segmental coordination of neuronal oscillators: synaptic mechanisms for uni-directional coupling during swimming in Xenopus tadpoles. *J Comput Neurosci* 13: 143–158, 2002.

Wenning A, Cymbalyuk GS, Calabrese RL. Heartbeat control in leeches. I. Constriction pattern and neural modulation of blood pressure in intact animals. *J Neurophysiol* 91: 382–396, 2004a.

Wenning A, Hill AA, Calabrese RL. Heartbeat control in leeches. II. Fictive motor pattern. *J Neurophysiol* 91: 397–409, 2004b.

Zelenin PV, Grillner S, Orlovsky GN, Deliagina TG. Heterogeneity of the population of command neurons in the lamprey. *J Neurosci* 21: 7793–7803, 2001.

Zelenin PV, Orlovsky GN, Deliagina TG. Sensory-motor transformation by individual command neurons. *J Neurosci* 27: 1024–1032, 2007.

Zelenin PV, Pavlova EL, Grillner S, Orlovsky GN, Deliagina TG. Comparison of the motor effects of individual vestibulo- and reticulospinal neurons on dorsal and ventral myotomes in lamprey. *J Neurophysiol* 90: 3161–3167, 2003.